CALPHAD: Computer Coupling of Phase Diagrams and Thermochemistry 68 (2020) 101713

Contents lists available at ScienceDirect

Calphad

journal homepage: http://www.elsevier.com/locate/calphad

On the complexity of solid-state diffusion in highly concentrated alloys and the sluggish diffusion core-effect

Cláudio G. Schön [a,*], Matheus A. Tunes [b], Raymundo Arróyave [c], John Ågren [d]

[a] Department of Metallurgical and Materials Engineering, Escola Politécnica da Universidade de São Paulo, Brazil
[b] Chair of Non-ferrous Metallurgy, Montanuniversitaet Leoben, Austria
[c] Department of Materials Science and Engineering, Texas A&M University, USA
[d] Materials Science and Engineering, Royal Institute of Technology, Sweden

ARTICLE INFO

Keywords:
Highly concentrated alloys
Sluggish diffusion
Cluster variation method
DICTRA

ABSTRACT

Diffusion paths in system V – Nb – W – Al in the highly concentrated region (*i.e.* as "High Entropy Alloys") are modelled using DICTRA code with commercial databases and with a new algorithm, based on the Cluster Variation Method (CVM). The DICTRA simulations, which produce realistic diffusion profiles, show that the diffusion path is non-linear. The CVM simulations, with parameters obtained by *ab initio* calculations, allow to investigate in an incremental way the effects of thermodynamics, of correlations and the role of the intrinsic diffusivities of the components. The results confirm the non-linear character of the diffusion path, and show that it is primarily driven by the complex thermodynamics characteristic of these alloys. When the intrinsic diffusivities are used, it is observed that the slowest diffusing species (in the present case, W) will constrain the whole diffusion process. This is likely the origin of the so called "sluggish diffusion" effect and it is of kinetic origin, bearing no relation with the configurational entropy.

1. Introduction

Highly concentrated alloys (HCA), usually referred to as High-entropy-alloys (HEA), belong to a class of new materials that brought to metallurgy a set of new concepts, results and methodologies which have potential to revolutionise its existing boundaries. It may thus be regarded as a new paradigm, in which the alloy design principles of conventional metallurgy are radically redefined. HCAs are typically synthesised with five or more substitutional alloying elements at (near-) equiatomic composition in contrast with the terminal solid solution concept that has dominated most of the metallic alloy paradigms used nowadays (such as Al- [1–4], Fe- [5,6], Ni- [7] and Zr-based alloys [8]). It should be mentioned though that some high-alloyed steels may actually also be termed HCA or HEA.

From the definition of HCAs, the conceptualisation of four core-effects are often mentioned in literature to be the underlying fundamental principles that are responsible for the differentiation of the HCAs relative to traditional terminal solid solutions [9–18]. These core-effects are summarised as follows:

The high-entropy effect: If all elements could dissolve in a single phase, the equiatomic condition maximises the Boltzmann's configurational entropy of that phase resulting in the minimisation of its Gibbs free energy. By this, the number of retained phases in the HCA solid solution after casting is significantly reduced as the maximum entropy stabilises a single solid solution phase at high temperatures [14,19–21]. Recent research investigated the influence of configurational entropy on the stability of a refractory HCA – the VNbTaMoW – and indicated that thermodynamic stabilisation in these alloys may be due to conflicting interactions (*i.e.* frustration) and not the configurational entropy maximisation [22].

Severe lattice distortion effect: As a HCA solid solution is composed of alloying elements with different atomic sizes, its crystal structure will suffer with severe crystal lattice distortion (Fig. 1). It has been reported that such lattice distortion effect raises the local free energy state of the HCA, thus modifying their physical metallurgy properties by impeding dislocation motion [23].

Cocktail effect: When different elements are mixed at equiatomic composition, as a result of mutual interactions between the elements, a synergistic effect takes place resulting that excess quantities within the alloy system are brought to their average values [24]. For example, it has been reported that the addition of light elements make the final alloy less dense [9,19]. In addition, by carefully controlling the addition of Al

* Corresponding author.
E-mail address: schoen@usp.br (C.G. Schön).

https://doi.org/10.1016/j.calphad.2019.101713
Received 20 August 2019; Received in revised form 12 November 2019; Accepted 14 November 2019
Available online 3 December 2019

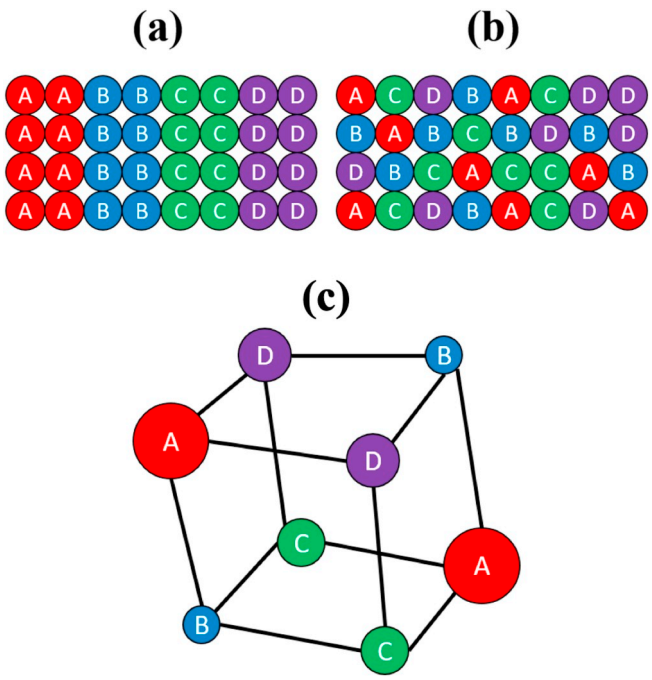

Fig. 1. The conceptualisation of HCAs: (a) a quaternary alloy in its ordered state, (b) a random solid solution after mixing of its constituents and (c) the resulting severe lattice distortion effect (Adapted from Murty et al. [13]).

into the CoCrCuFeNi HCA, significantly hardening was observed. This is presumed due to the cocktail effect, as stronger bonding will be established between Al and the other elements with larger atomic sizes [9,19].

Sluggish diffusion effect: It was proposed by Yeh et al. [10] and Cheng et al. [25] that both phase transformation kinetics and atomic diffusion are slower in HCAs when compared with conventional diluted solid solution alloys [9]. It has been reported that such sluggish diffusion effect acts in order to promote the nucleation of nanometre-sized precipitates of HCAs even in a cast state [26–28]. As a direct application, this effect has been also reported to mitigate either the generation and evolution of point and extended radiation-induced defects [12,29,30], thus leading to HCAs with superior radiation resistance as the elemental composition parameter can be used to produce alloys with controllable defect mobility and migration pathways [31].

These core-effects are often listed as the underlying factors behind the superior and unique set of properties that such HCAs are exhibiting when experiments are carried out in several branches of material sciences [12–14,20,32–38]. However, from a fundamental point of view all these core effects may be questioned. In most cases the experimental observations may be well explained within established theories. Currently, there is a lack of studies that investigate such core-effects on a fundamental basis and this is of paramount importance for development of the field. Recent criticism on the sluggish diffusion [39] and on the high-entropy core effects [22] have indicated that some of the constitutive hypothesis on the theory of HCAs require deeper investigations.

1.1. The sluggish diffusion core-effect: Quo vadis?

From a fundamental point of view this effect is contrary to what would be expected because it is well-known that ordering, *i.e.* the opposite to high entropy, strongly retards diffusion. Nevertheless, Tsai et al. [40] concluded that diffusion is more sluggish in HCAs than in conventional alloys. They investigated atomic diffusion in a quinary HCA – the CoCrFeMnNi – by using a quasi-chemical model in order to simplify the calculations within the multicomponent system. To do so, the authors made the following assumptions: (i) the CoCrFeMnNi HCA is a near-ideal solid solution; (ii) it is feasible to study multicomponent diffusion by using a binary diffusion couple model; and (iii) minor alloying elements within the couple will not diffuse (or their diffusion is negligible). Criticism on the work by Tsai et al. was later presented by Paul [41]. In his paper, the latter author commented on the impossibility of estimating diffusion coefficients in a five-component system by simply using conventional methods. In addition, as the intrinsic diffusion coefficients were unknown, the average diffusion coefficients (as calculated by Tsai et al. [40]) are of limited physical significance. Although based on a faulty model [41], the calculations by Tsai et al. [40] identified "sluggishness" in the diffusion parameters of the quinary HCA which was attributed to the disorder of the lattice as promoted by the maximisation of the configurational entropy. According to these authors, such sluggish diffusion results into *"(…) greater fluctuation of lattice potential energy* [that] *produces more significant atomic traps and blocks, leading to higher activation energies"* [40].

Recent works investigated sluggish diffusion using an experimental perspective. By annealing diffusion couples of the CoCrFeMnNi, CoFeMnNi, CoCrFeNi and CoCrMnNi HCAs at temperatures up to 1350 K, Dabrowa et al. [39] obtained experimental values for diffusivity in these multicomponent systems and no evident signs of diffusion retardation were observed. The authors also pointed out that sluggishness only occurred in alloys with significant Mn content and it was independent on the number of alloying elements of the HCAs. In this sense, the sluggishness observed in the Mn-containing HCAs indicates that the sluggish diffusion in these concentrated alloys should be treated as a consequence of specific elemental compositions and cannot be extended to the general class of HCAs [39]. Similarly, by studying the effects of ion irradiation *in situ* within a transmission electron microscope in either a quaternary HCA – the FeCrMnNi – and an homologous austenitic stainless steel (AISI-348) with same elements as major solutes, Tunes et al. [42] observed that the nucleation and growth of inert gas bubbles as well as the development and accumulation of radiation-induced crystalline defects were very similar in both alloys. If sluggish diffusion acted to retard the development and evolution of defects in the FeCrMnNi HCA, the effect is in the lowest limit of experimental evidence. The discrepancy between experimental evidence and theoretical/computational works addressed on the sluggish diffusion core-effect indicates that the atomic diffusion in HCAs is a complex phenomenon and deserves further investigation at a fundamental level.

1.2. On the role of diffusion in materials science and technology

Diffusion, and in particular, solid state diffusion, plays a fundamental role in materials science and technology. Many phase transitions observed in iron, aluminum, titanium and copper alloys are diffusion-controlled, meaning their kinetics are defined by the diffusion rate of the different species. This has a strong impact in processing. Heat treatment, for example, is nothing more than a procedure to control (and in some cases, to suppress) phase transformations, and hence, it relies on selectively controlling at which rate the different species in the alloy diffuse [43–46]. The impact of diffusion in technology, however, is not only limited to its intentional use in heat treatment. In some occasions materials may operate in conditions in which unintentional diffusion takes place, sometimes with severe consequences [47–51]. Multi-component diffusion is a complex process even in conventional (meaning dilute) alloys, and require proper modeling [45,52]. It is observed, for example, that even trace amounts of alloying elements in steels may have strong impacts over precipitation kinetics [53], this shows that the proper understanding of diffusion in the highly concentrated composition range is vital for the development of this class of materials.

The present work aims to analyse diffusion in multicomponent alloys (in the concentrated composition range). This will be done by simulating the diffusion paths (i.e. the path in composition space which is produced in a diffusion couple) in system V – Nb – W – Al, with the body centered

cubic disordered (A2) structure. This will be done by simulating a diffusion couple with the well-established DICTRA code, using commercial mobility and thermodynamics databases. Second, a new algorithm based on the Cluster Variation Method (CVM) will be presented. This algorithm allows the simulation of the diffusion path using *ab initio* data, and using an incremental procedure as well, in which first the effect of thermodynamics is simulated, then the effect of correlations (using adapted Manning's mobilities [54]), and then finally including self-diffusivities of the elements, to understand how the different aspects of diffusion affect the process.

2. Methodology of calculation

2.1. Choice of system

System V – Nb – W – Al was selected for this investigation, based on previous results obtained by some of the present authors [55]. Based on *ab initio* calculations it is concluded that the disordered BCC phase (A2) is stable above ≈ 1100 K in the highly concentrated composition range, and that it is characterized by very large short-range order (SRO) parameters and activity coefficients for the four species, which enhance the non-linear effect of thermodynamics (here understood as the composition dependence of chemical potentials, as discussed in Ref. [22]) in these compositions. The temperature of $T = 1200$ K has then been selected for the present simulations as this avoids the presence of long-range ordered states (LRO) while still keeping large deviations from the ideal thermodynamic behavior. The choice of this BCC system was made due to the fact that the present CVM code, in this approximation, models BCC systems and to select elements which have a stable BCC ground state, without interference of magnetism.

The simulated "diffusion couples" correspond to the initial contact of two infinite bars of highly concentrated alloys, one with composition $V_{0.2}Nb_{0.4}W_{0.2}Al_{0.2}$ and the other with composition $V_{0.25}Nb_{0.25}W_{0.25}Al_{0.25}$, the geometry of the system is assumed to be unidimensional.

2.2. DICTRA simulations

In irreversible thermodynamics the diffusional flux j_i of a species i in the lattice-fixed frame of reference can be expressed as a linear combination of the thermodynamic forces, *i.e.* the gradients of the thermodynamic potentials. In a system with q components one thus writes, under isobarothermal conditions Eqn 1:

$$j_i = -\sum_{j=1}^{q} L_{ij} \nabla \mu_j \tag{1}$$

For a substitutional solution DICTRA [56] is based on the so-called vacancy mechanism, *i.e.* diffusion occurs by an atom jumping to a neighbouring vacant site leaving a vacancy behind. Neglecting correlation effects [54] the L_{ij} matrix expressed in the lattice-fixed frame of reference becomes diagonal and introducing atomic mobilities M_i the flux equation becomes Eqn 2

$$j_i = -c_i M_i \nabla \mu_i \tag{2}$$

where c_i is the local concentration of i, *i.e.* the number of mole of i per unit volume and M_i the atomic mobility of i. It should be emphasized that this model is by no means restricted to dilute solutions and in principle it is able to handle any number of components in any composition range. Transforming to other frames of reference, *e.g.* the number-fixed frame of reference, introduces new set of forces and of diagonal elements in the corresponding L matrix. The accuracy of the calculated flux then depends on how well the mobilities represent the experimental data. Usually it is found that the mobilities are functions of the local composition.

The flux equation is then combined with conservation of species and the resulting set of partial differential equations solved with the Finite-element method.

Simulations were performed for the diffusion couple and temperature defined in the previous section using DICTRA as available in Thermo-Calc version 2019a. The commercial TCFE9 and MOBFE4 databases were used for the thermodynamic and diffusional properties, respectively. In the present case the MOBFE4 database is based on CALPHAD assessment of experimental data for binary and ternary alloys. Gaertnet et al. [57] criticise the use of these databases, but one has to consider that the kinetics of the process is not the focus of the present work, so their use is justified.

The simulations were performed for a total size of the diffusion couple of 200 μm and a time of 5 h. This time is short enough to prevent any impingement effects and the behaviour is parabolic. A double geometric grid with 101 points and geometric coefficients of 0.97 and 1.03, was used.

2.3. Cluster variation method algorithm

The cluster variation method (CVM) calculations are performed in the irregular tetrahedron approximation for the BCC lattice. Details of the basic formalism are found in previous publications by some of the authors [22,55]. Here only the details of the new algorithm will be described. The interested reader should consult the original references for details of this part of the methodology. Energy parameters are taken from VASP *ab initio* simulations described in Ref. [55].

The new algorithm, dubbed **dpath4**, is written in C++ (standard ISO C++11 is used, but the code can be easily ported for other C++ standards). Following the inherent Object Oriented Programming (OOP) philosophy of C++ the algorithm uses two base classes, named **cluster** and **bcc_it**. Object **cluster** provides a dynamic allocated memory array which stores the cluster probabilities, and the low-level programming methods used to deal with this probability distribution. Class **bcc_it** is derived from **cluster** and its object provides the description of a irregular tetrahedron CVM model, including the tetrahedron probability distribution, the energy matrix, all sub-cluster probabilities and the methods used to perform a CVM calculation using, for example, the Natural Iteration Method (NIM) [58].

A particular method of **bcc_it** was designed for the present simulations. This sub-algorithm is named **seek_comp()** and allows to find the chemical potential set $\{\mu_i^*\}$ corresponding to a given composition set $\{x_i\}$ (i = V, Nb, W). This is done by a bipartition algorithm and relies on the fact that function $\mu_i^*(x_i)$ is crescent (that is $d\mu_i^* > 0 \Rightarrow dx_i > 0$ and *vice-versa*). This is strictly valid only in thermodynamic stable states and it is predicted that this algorithm may fail to converge if the thermodynamic variables lead to a stable heterogeneous state. All present calculations were performed in situations in which only the A2 phase (and a single A2 phase) is stable, so the algorithm was observed to converge in all occasions.

The bipartition algorithm was chosen because it is inherently stable, in the sense that any initial condition leads to a solution. This is necessary due to the non-linear character of functions $\mu_i^*(x_i, x_j, \ldots)$ which prevent the use of more efficient linearization techniques (for example, Newton-Raphson). This leads, however, to a slow converging code. Although the algorithm is stable, it is also observed that it is subject to dynamic chaos, since the number of iterations for convergence (assuming a constant converging radius) is strongly dependent on the initial conditions, and in some cases they may lead to very large number of iterations.

The present algorithm is written to work with a quaternary system, but this is not a limitation of the algorithm itself, it was only a strategic decision by the authors. The codes are published under the GNU General Public Licence v. 3.0 (and the source codes are included as supplemental material of this manuscript).

Fig. 2 shows a schematic representation of the **dpath4** algorithm. It

starts by defining two **bcc_it** objects (A and B) and an array of cells, which stores the local composition and chemical potential. Cell "0" contains the data of the initial composition of the "diffusion couple" and their contents (that is, composition and chemical potentials) are kept constant during the entire simulation. At each iteration a new cell is created. The composition of this cell is updated using the kinetic equations (to be discussed in the sequence) and **seek_comp()** is ran, to find the new values of chemical potentials for this cell. The algorithm is then reiterated, each time creating a new cell. Diffusion takes place between the last cells of both object, as well as inside the objects, between the already calculated cells (the atomic fluxes, in these cases are generally much smaller than the one observed between the last cells in the respective objects).

2.4. Kinetic laws for the CVM calculation

We follow the formalism developed in Ref. [22], based on irreversible thermodynamics [59], to write the relation between the diffusion flux of component i, j_i, and the generalized forces $\nabla(\mu_i^* - \mu_{Al}^*)$ Eqn 3:

$$j_i = -\sum_j M_{i,j}\nabla\left(\mu_j^* - \mu_{Al}^*\right) \tag{3}$$

for $(i,j) =$ V, Nb, W. Here μ_i^* represent the chemical potential of components i in a special reference system defined by condition:

$$\sum_{n=\mathrm{V,Nb,W,Al}} \mu_n^* = 0 \tag{4}$$

This Eqn 4 ensures that the mass conservation constraint is met in the calculations. In modelling diffusion this formalism neglects the role of vacancies, which are not included in the model. Hence the present calculations correspond, strictly speaking, to a direct substitution diffusion model.

Coefficients $M_{i,j}$ represent the generalized mobilities of the components, the diagonal terms represent the effect of the gradient of chemical potential of a given component over its own flux, while the off-diagonal terms represent the effect of the gradient of chemical potential of a given component over the flux of a second, different, component. The present calculations will probe the different contributions to the diffusion flux by defining different mobilities, as it will be discussed further on in this section.

The diffusion couples are modelled as two blocks of alloy, named A and B, of different concentrations, with unit cross section. The gradient, hence, is one dimensional. Assuming that space is discretized using a constant length $d\ell \equiv \Delta\ell$, we may approximate the chemical potential gradients as Eqn 5:

$$\nabla\ \mu_i^* - \mu_{\mathrm{Al}}^*) \approx \frac{\Delta\ \mu_i^* - \mu_{\mathrm{Al}}^*)}{\Delta\ell} \tag{5}$$

During the simulation, cells 0 in both blocks correspond to the initial concentration of the block and are kept constant throughout the simulation. They act, therefore, as particle reservoirs for the remaining cells. Table 1 shows the composition and the corresponding chemical potentials used for the simulated diffusion couple.

Every further cell created by the algorithm has its concentration at each iteration updated by calculating Eqn 6:

$$\mathrm{d}x_i = j_i \mathrm{d}t \qquad (i = \mathrm{V, Nb, W}) \tag{6}$$

where dt is the time step chosen for the simulation. This is possible since the simulations are performed in the framework of the rigid lattice approximation (*i.e.* the molar volume is assumed constant and equal for all components).

Initial trials using a constant time interval lead to very large composition changes at the beginning of the simulation, therefore it was decided to use a variable time step, starting at 100 s, multiplying by 10 every 500 iterations. A "time" is attributed to each cell (meaning the time in which it was created) and an arbitrary distance is calculated as the square root of this time. Since the kinetics of the process is not the main focus of the present work, this distance will be presented in the form of arbitrary units (a.u.).

The first simulation probes the effect of thermodynamics on diffusion, using constant mobilities. Since the width of the cell is arbitrary, we define the fluxes directly (Eqn 7):

$$j_i = -\frac{1}{k_B T} \times 10^{-6} \times \Delta\ \mu_i^* - \mu_{\mathrm{Al}}^*) \quad \mathrm{s}^{-1} \qquad (i = \mathrm{V, Nb, W}) \tag{7}$$

In this case the diffusion flux will respond only to the difference of chemical potentials between neighbouring cell, producing a "natural" diffusion path. Observe that if the alloy was indeed behaving as an ideal solution, this diffusion path would be a straight line in the composition space.

The second simulation is designed to investigate the role of correlations in defining the diffusion path. We start with the model developed by Manning [54] to consider the effect of vacancy wind on the mobilities for multicomponent alloys (Eqn 8a):

$$M_{i,i} = \frac{x_i D_i^* C}{k_B T}\left[1 + \frac{2x_i D_i^*}{\Xi_0 \sum_{m=\mathrm{V,Nb,W,Al}} x_m D_m^*}\right] \tag{8a}$$

and

$$M_{i,j} = \frac{2x_i x_j D_i^* D_j^* C}{k_B T \Xi_0 \sum_{m=\mathrm{V,Nb,W,Al}} x_m D_m^*} \tag{8b}$$

with constant C defined as (Eqn 8c):

$$C = \sum_m x_m \tag{8c}$$

In these cases the summations in i, j and m run over all components.

In these expressions, constant Ξ_0 is a lattice-dependent constant which takes the value 5.33 for BCC lattices (as in the present case). Constants D_k^* correspond, in Manning's description, to the tracer diffusivities of the respective components, which, for this simulation will be set to 10^{-5} s^{-1} for all components (as in the first simulation, the arbitrary width of the cell is already accounted for in this value. In writing equations (8a) and (8b) use was made of the rigid lattice approximation, to express components concentrations as molar fractions.

For the present purposes these expressions will be adapted. First, we observe that both equations contain a term involving a product of molar fractions. In examining the original deduction by Manning [54] we observe that the author used the hypothesis that atom pairs were uncorrelated. This product, however, is an approximation for the nearest neighbor pair probability $\rho_{i,j}^{\alpha\gamma}$, which can be directly obtained from the CVM calculation (see, for example, ref. [22]). In addition, the present direct substitution model contains no vacancies, so that the flux of aluminum linearly depends on the flux of the other components, therefore we write Eqn 9a:

$$M_{i,i} = \frac{x_i D_i^* C'}{k_B T} + \frac{2\rho_{i,i}^{\alpha\gamma}\ D_i^*)^2 C'}{k_B T \Xi_0 \sum_{m=\mathrm{V,Nb,W}} x_m D_m^*} \tag{9a}$$

and Eqn 9b

$$M_{i,j} = \frac{2\rho_{i,j}^{\alpha\gamma} D_i^* D_j^* C'}{k_B T \Xi_0 \sum_{m=\mathrm{V,Nb,W}} x_m D_m^*} \tag{9b}$$

with Eqn 9c

$$C' = \sum_{i=\mathrm{V,Nb,W}} x_i \tag{9c}$$

In these cases, the summations over i, j and m run over the set V, Nb, W.

In the third simulation, realistic values for the tracer diffusion

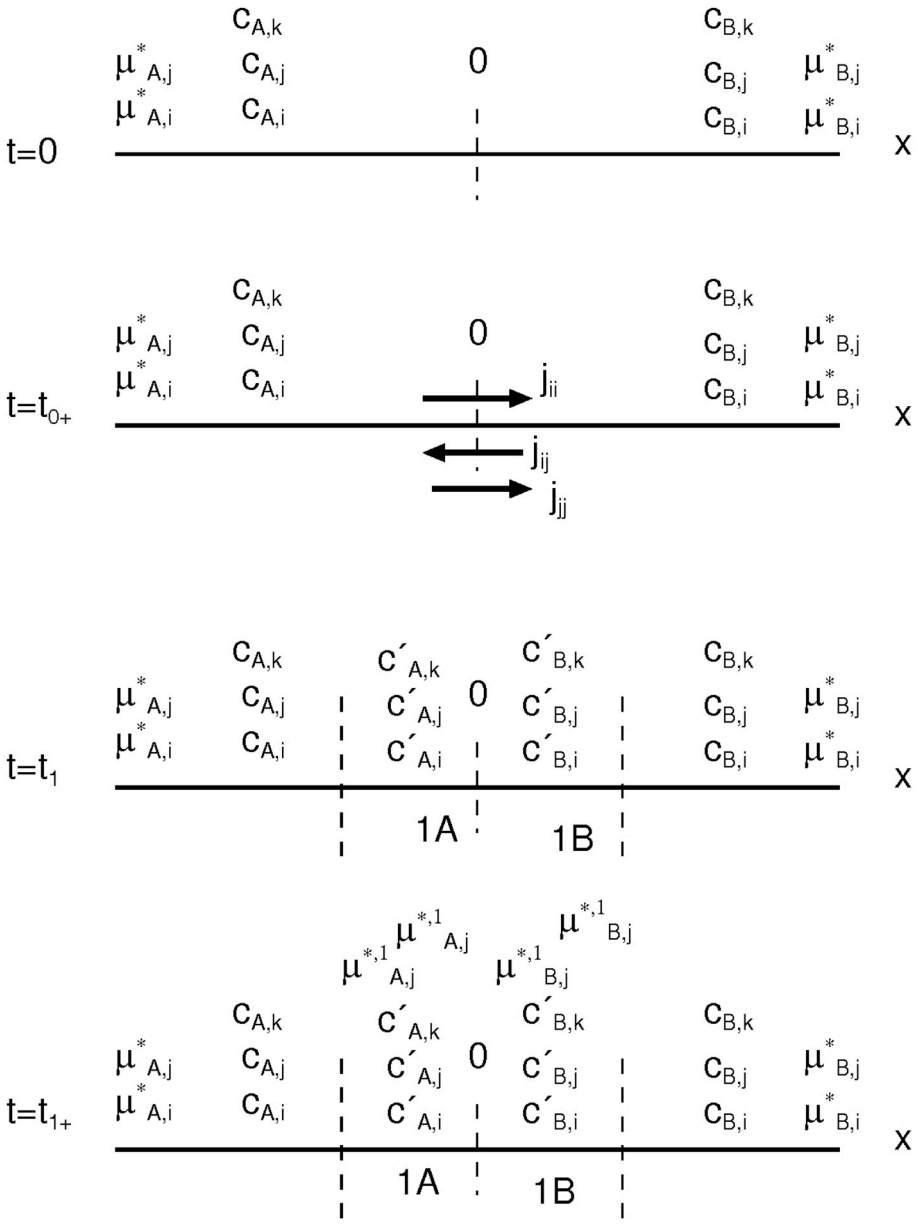

Fig. 2. Schematic representation of the **dpath4** algorithm.

Table 1
Initial values for the simulated diffusion couple (and corresponding values for cell 0 in all simulation). Chemical potentials expressed in units of k_B $K \equiv$ 8.3145 J mol^{-1}.

Block	x_V	x_{Nb}	x_W	x_{Al}	μ^*_V	μ^*_{Nb}	μ^*_W	μ^*_{Al}
A	0.20	0.40	0.20	0.20	−172.961	663.583	631.058	−1121,68
B	0.25	0.25	0.25	0.25	−653.410	−128.820	922.210	139.980

constants of V, Nb and W are used together with Equations (9a) and (9b), allowing to probe all three contributions to diffusion (thermodynamic effects, correlation effects and proper mobility of atoms).

Here one word of caution is necessary. As stated before, the present diffusion model corresponds to a simple substitution mechanism. It is very difficult, perhaps impossible, to estimate mobilities for this mechanism, and even if it were possible to find values, these would result in very slow diffusivities, turning the whole simulation unrealistic. Since the aim of the present work is to discuss the effect of the three contributions to diffusion in the formation of a realistic diffusion path, and not on the kinetics of diffusion itself, it was decided to select experimental tracer diffusivities measured/estimated from self-diffusion and inter-diffusion experiments in V, Nb and W. These experimental values, of course, refer to a vacancy-mediated process, as it is usual for metallic disordered alloys. Naturally, vacancies could be included in the model, but this poses difficulties which need to be carefully considered [60], and are therefore outside the scope of the present work, hence the present approximation is justified. Also, as Gaertner et al. [57], diffusivities may be composition-dependent and so the self-diffusivities should be determined as close to the actual compositions of the

diffusion couple. Since the intention here is just to show how differences in the mobilities affect the diffusion path, this will be neglected in the present work.

For vanadium we use proper tracer diffusion data measured by Peart [61]. This author studied diffusion of V^{48} isotopes in vanadium single crystals, obtaining an expression[1] for the tracer diffusion constant valid for the temperature range between 1153 K and 1626 K as (Eqn 10)

$$D^*_V(T) = (0.36 \pm 0.02)\exp\left(-\frac{308200 \pm 1400}{k_B T}\right) \mathrm{cm^2 s^{-1}} \quad (10)$$

Applying this to the temperature of the simulation results in $D^*_V = 1.3895 \times 10^{-14} \mathrm{cm^2\ s^{-1}}$.

In the case of Nb, we use the results reported by Einziger et al. [62], which were obtained by the radiotracer method, using Nb^{95} isotopes in single crystalline bulk samples of Nb. Measurements ranged from 1354 K to 2695 K, which means that the temperature of the simulations is below the measurement range. The authors reported an expression for the tracer self-diffusivity of Nb in the form of a double exponential fit (Eqn 11):

$$D^*_{Nb}(T) = \left[(8 \pm 3) \times 10^{-3}\right]\exp\left(-\frac{349300 \pm 8700}{k_B T}\right) + \\ +(3.7 \pm 0.03)\exp\left(-\frac{438000 \pm 970}{k_B T}\right) \mathrm{cm^2 s^{-1}} \quad (11)$$

Applying this equation for the temperature of the simulation results in $D^*_{Nb} = 5.3307 \times 10^{-18} \mathrm{cm^2\ s^{-1}}$.

Finally the results of Mundy et al. [63] for tungsten are selected. These authors used the radiotracer method in single crystals of W, with W^{187} as active isotope. Measurements ranged from 1705 K to 3409 K, which is well above the temperature of the simulation. The expression for the tracer self-diffusivity of W is (Eqn 12):

$$D^*_W(T) = 0.04^{0.17}_{0.01}\exp\left(-\frac{521000 \pm 50000}{k_B T}\right) + \\ +46^{136}_{16}\exp\left(-\frac{666000 \pm 60000}{k_B T}\right) \mathrm{cm^2 s^{-1}} \quad (12)$$

The extrapolated value for the tracer diffusivity of W at 1200 K is, therefore, $D^*_W = 8.3926 \times 10^{-25} \mathrm{cm^2\ s^{-1}}$.

In the case of this simulation a value of $\Delta\ell$ was selected, corresponding to 0.1 μm ($\equiv 10^{-7}$ cm).

3. Results and discussion

3.1. DICTRA simulations

The DICTRA simulations result in concentration profiles, i.e. c_i as functions of distance and time for each species *i*. In ternary systems, i.e. $C = 3$ there are only two independent concentration variables. It is then custom to plot the concentration of one species as a function of the composition of another species. At a given time such a plot results in a curve joining the composition of one side of the diffusion couple with the other side. Such a curve is called the diffusion path. For an infinite diffusion couple the process is parabolic, i.e. the concentration profiles may be expressed as functions of the single variable distance/time. Then information from all different times fall on a single curve when the diffusion path is plotted.

In the present case $C = 4$ and there are 3 independent concentration variables, *i.e.* the diffusion path will be a curve in a 3-dimensional diagram. An example is shown in Fig. 3.

It is interesting to see that the behaviour is quite complex and by no means linear. It should be emphasized that the predicted behaviour is just a consequence of combining the thermodynamic and mobility information without adding any special "entropic" in addition to what is included in the normal thermodynamics.

3.2. CVM simulations

3.2.1. Effect of thermodynamics

Fig. 4 shows the diffusion path produced in the simulation in which only contributions of thermodynamics are included (Equation (7)), after 1700 iterations of the algorithm. As these curves show, the diffusion path is far from a straight line in the composition space, proving the complex nature of diffusion in these alloys, as already observed in the case of the DICTRA simulation.

Fig. 5 shows the corresponding composition profiles. As already mentioned, the "distance" expressed in this figure corresponds to an arbitrary length scale.

As observed, the composition profiles are considerably non-linear. For example, both V and W present uphill diffusion in the initial part of the profiles, resuming a "normal" behavior in the later stages. The profile for Al, on the other hand, shows a strong composition change in the initial stages, starting a slow stage of uphill diffusion in the intermediate range of the diffusion zone. Even Nb, which shows a monotonic reduction of content from the high content block towards the low content block, presents a profile which is far from usual and not characteristic, for example, of binary diffusion. In general, we may conclude that all components of the alloy participate in the diffusion process in a complex manner.

It is necessary to stress again: these are the effects of thermodynamics alone in the diffusion process. In binary alloys this effect is limited to either an acceleration, or to a depression of the diffusion flux, due to the thermodynamic factor of diffusion [64], but in multicomponent alloys the effects are much richer, leading to these non-linear diffusion paths.

3.3. Effect of correlations

When correlations are introduced via the adapted Manning's formalism, we observe only a small perturbation from the previous diffusion path, as depicted in Fig. 6. In the present case the simulation converged with 1500 iterations.

Fig. 7 shows the concentration profiles produced in the second simulation (using the adapted Manning's formalism). The results are again compared with the ones obtained in the first simulation (thermodynamics only). In this figure the distance scale was set so that it

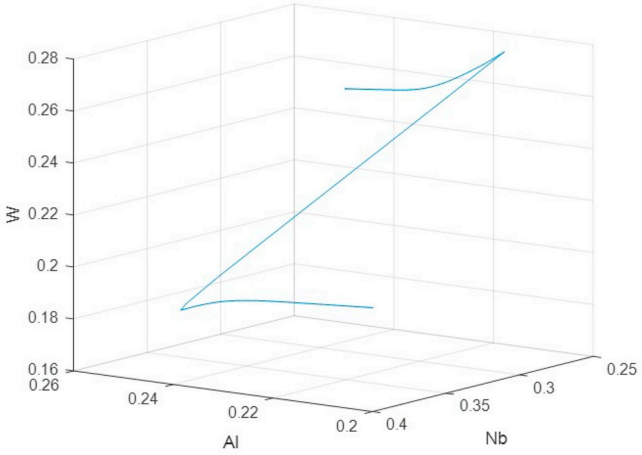

Fig. 3. Diffusion path calculated with DICTRA for the diffusion couple. The Al, Nb and W content are used as axis variables. The V content is thus a dependent variable.

[1] The original activation enthalpy for the three elements was reported in either kcal mol^{-1} or eV $atom^{-1}$, here the values were converted in J mol^{-1}.

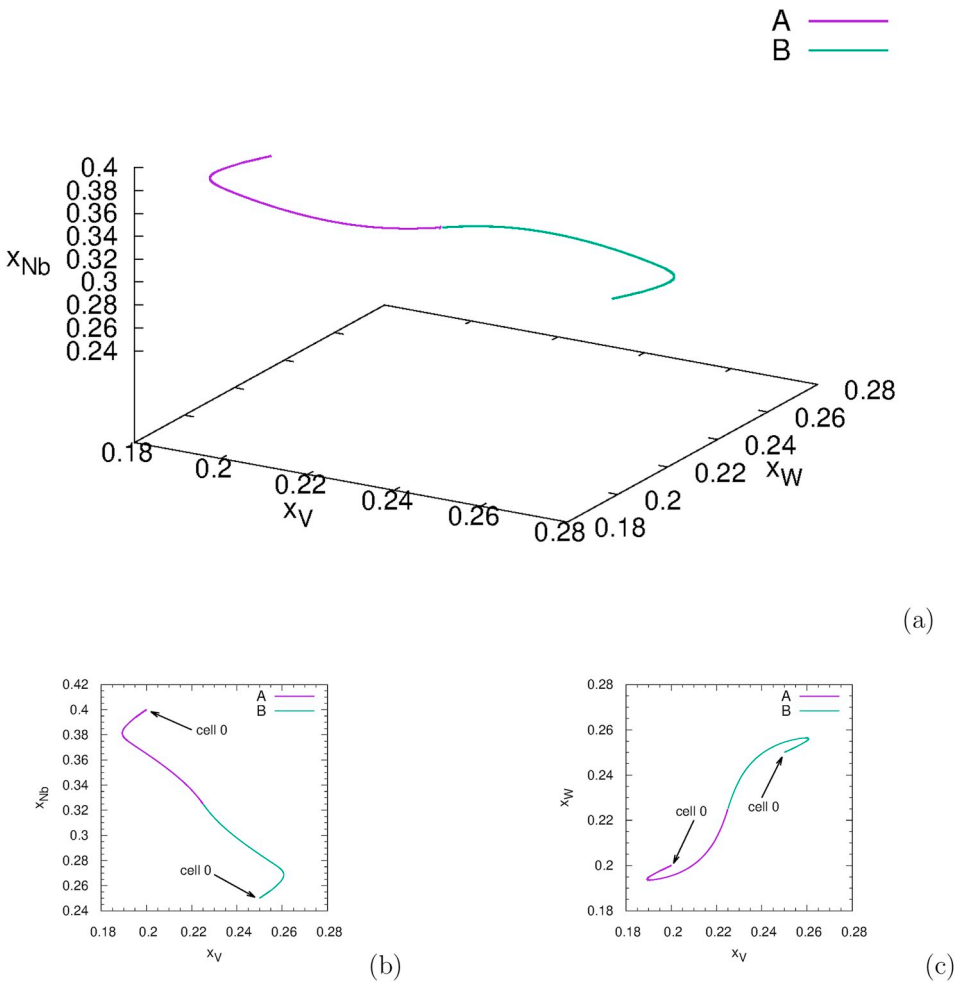

Fig. 4. Diffusion path produced for the diffusion couple using the model in which only thermodynamic contributions for the diffusion are included. (a) panoramic view, (b) - projection in the V – Nb plane and (c) - Projection in the V – W plane.

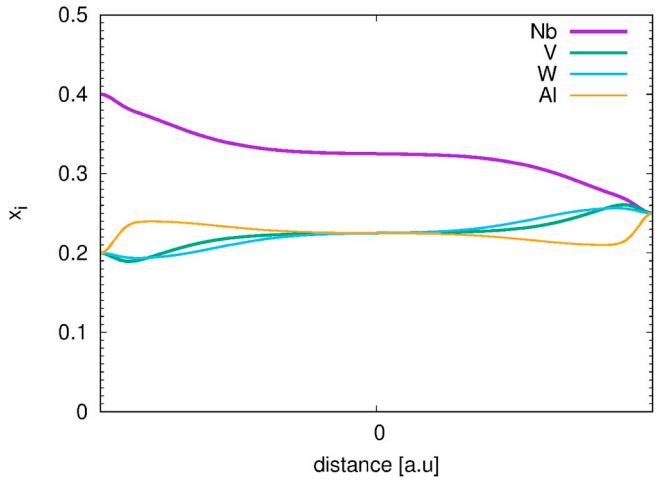

Fig. 5. Composition profiles in the simulated diffusion couple, corresponding to the diffusion path of Fig. 4.

presents the whole diffusion zone in both cases, but the kinetics in both cases is considerably different, so that the comparison should be made with care.

In general, the introduction of correlation effects lead to smoother concentration profiles.

The effect of correlations, according to this formalism, is very weak. This could be anticipated by analysis of Equations (9a) and (9b), since the diagonal mobilities are roughly proportional to x_i, while the off-diagonal mobilities are proportional to $\rho_{i,j}^{\alpha\gamma}$, which are of the order of $(x_i)^2$. As the molar fractions are fractions of the unity, we conclude that the effect of correlations represents, according to this formalism, a small perturbation over the effect of thermodynamics.

3.4. *Effect of the tracer diffusivities*

The last simulation is produced using the previously derived tracer diffusivities. First we observe that there are large differences between the diffusivities of the three components (several orders of magnitude when compared). In this sense, vanadium is a fast diffuser, niobium is an intermediate diffuser and tungsten is a slow diffuser. These differences are so large that numerical problems were found in the simulation, which prevented running the simulation to the end. The results shown in Fig. 8 corresponds to 700 iterations of the algorithm (and a total time of 226500 s).

In this simulation we observe that vanadium is rapidly diffusing in uphill diffusion (according to the thermodynamic effect) up to a certain concentration, and then it stops diffusing. As a result of being a fast diffuser, the vanadium concentration changes until the combination of potentials and mobilities results in null flux. Further diffusion of vanadium will be then constrained to follow the diffusion of Nb, and this will be constrained to follow the diffusion of W. In other words, the kinetics of diffusion is constrained by the slowest diffusing species. This is in

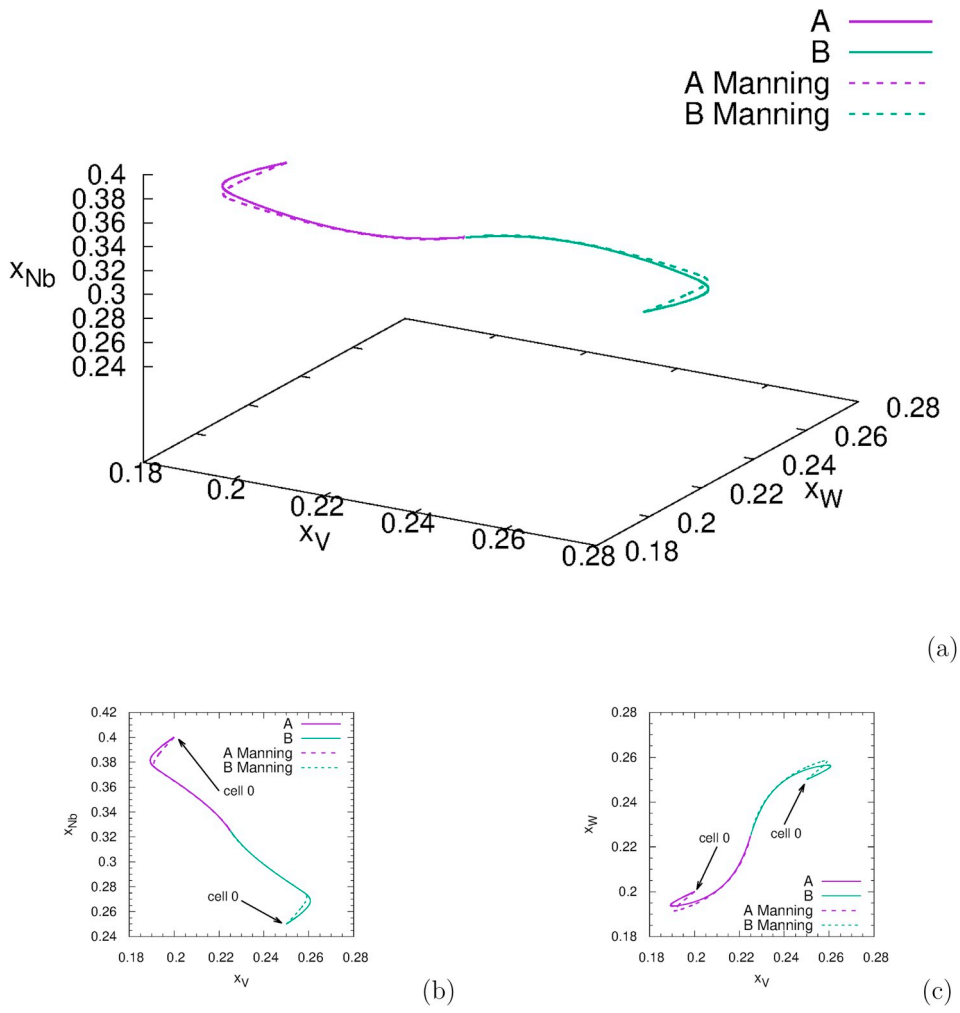

Figure 6. Diffusion path produced for the diffusion couple using the adapted Manning's formalism model (dashed line), compared with the model in which only thermodynamic contributions for the diffusion are included (full line). (a) panoramic view, (b) - projection in the V – Nb plane and (c) - Projection in the V - W plane.

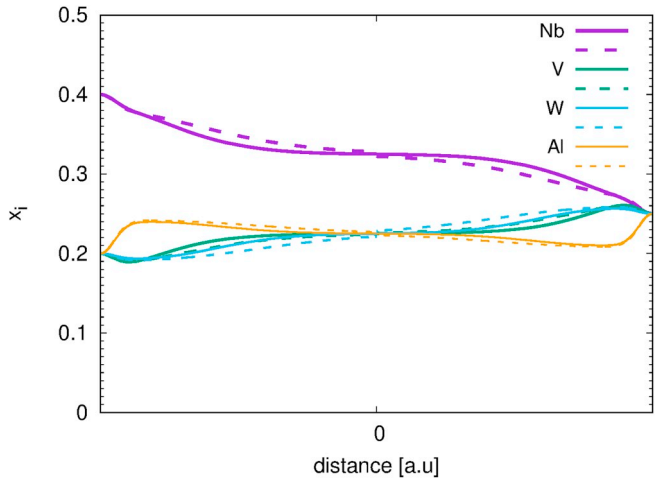

Fig. 7. Concentration profile obtained in the simulations with the adapted Manning's mobilities (dashed lines) compared with the results of the first simulation (thermodynamics only). The length scale of the simulations was adjusted so that in both cases the entire diffusion zone is depicted.

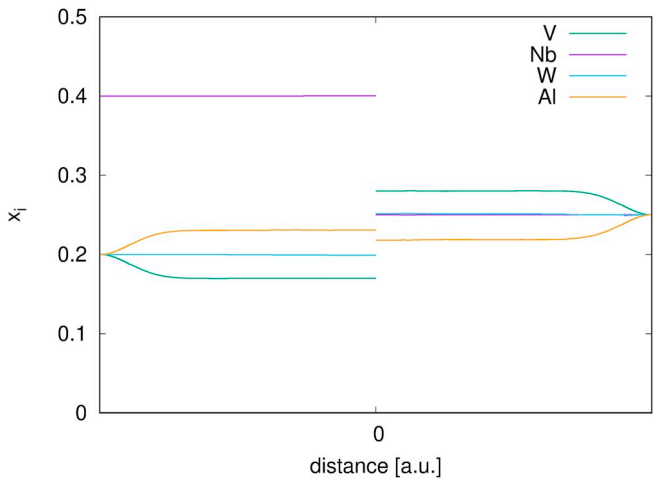

Fig. 8. Composition profile produced after 700 iterations of the algorithm using the tracer mobilities of V, Nb and W.

agreement with the findings of Dabrowa et al. [39], who associated sluggish diffusion in the investigated high entropy alloys to a particular species (in their case, Mn), which is fast-diffusing. In this case, the role of

Mn would be similar to that of V in the present simulation. It diffuses fast reducing the chemical potential gradients. Further diffusion of Mn requires changes in the chemical potential profiles due to the diffusion of the slower-diffusing components, hence, as suggested here, the slow-diffusing elements constrain the whole diffusion process.

In the opinion of the present authors, this is the origin of sluggish diffusion in HCAs reported in the literature. The multicomponent character of the highly concentrated alloys allows sufficient flexibility in the diffusion fluxes, so that one slow diffusing species can control the entire diffusion process. Evidently, this has no influence of disorder in the lattice, it is just a kinetic effect.

4. Conclusions

As the simulations of the present work demonstrate, diffusion in multicomponent alloys, particularly in the highly concentrated composition region, is considerably complex. Diffusion paths are non-linear and this is primarily driven by the complex thermodynamics which are characteristic of these systems.

A wide variety of phenomena like uphill diffusion are common and may set on and off during a single diffusion experiment for any component. In particular, minority components in a diffusion pair cannot be disregarded, since they participate actively in the solid-state diffusion process.

Correlation effects, at least as the ones accounted for in the present calculation formalism, produce only a small perturbation of the diffusion path produced by thermodynamics alone, hence, the largest effect is produced by thermodynamics.

If realistic diffusivities are used in the simulation, it turns out that the slowest diffusing species will constrain the whole diffusion process, therefore, sluggish diffusion exists, but as a kinetic effect, without relation to the lattice disorder. Such effects have nothing to do with the ideal entropy of mixing. On the contrary short range ordering effects, i.e. the opposite to disorder, will slow down diffusion.

Acknowledgements

CGS acknowledges the financial support by the Brazilian National Research, Technology and Innovation Council (CNPq, Brasília, Brazil) under project 308565/2018-5 and by the São Paulo State Research Funding Foundation (FAPESP, São Paulo, Brazil) under project 2018/22114-1. MAT would like to thank assoz. Prof. Dipl.-Ing. Dr.mont. Stefan Pogatscher (MU Leoben) to support his post-doctoral research under the European Research Council (ERC) excellent science grant "TRANSDESIGN" through the Horizon 2020 programme under contract number 757961. RA acknowledges the National Science Foundation through Grant No. 1729350.

Appendix A. Supplementary data

Supplementary data to this article can be found online at https://doi.org/10.1016/j.calphad.2019.101713.

References

[1] L.F. Mondolfo, Aluminum Alloys: Structure and Properties, Elsevier, 2013.
[2] S. Pogatscher, H. Antrekowitsch, H. Leitner, T. Ebner, P.J. Uggowitzer, Mechanisms controlling the artificial aging of Al–Mg–Si alloys, Acta Mater. 59 (9) (2011) 3352–3363.
[3] L. Stemper, B. Mitas, T. Kremmer, S. Otterbach, P.J. Uggowitzer, S. Pogatscher, Age-hardening of high pressure die casting AlMg alloys with Zn and combined Zn and Cu additions, Materials & Design, 2019, p. 107927.
[4] J.A. Österreicher, M. Kumar, A. Schiffl, S. Schwarz, G.R. Bourret, Secondary precipitation during homogenization of al-mg-si alloys: influence on high temperature flow stress, Mater. Sci. Eng. A 687 (2017) 175–180.
[5] H. Bhadeshia, R. Honeycombe, Steels: Microstructure and Properties, Butterworth-Heinemann, 2017.
[6] L. Scheer, Was Ist Stahl? Springer, 1941.
[7] R.C. Reed, The Superalloys: Fundamentals and Applications, Cambridge university press, 2008.
[8] D.O. Northwood, The development and applications of zirconium alloys, Mater. Des. 6 (2) (1985) 58–70.
[9] M.-H. Tsai, J.-W. Yeh, High-entropy alloys: a critical review, Mater. Res. Lett. 2 (3) (2014) 107–123.
[10] Y. Jien-Wei, Recent progress in high entropy alloys, Ann. Chim. Sci. Mat. 31 (6) (2006) 633–648.
[11] J.-W. Yeh, Alloy design strategies and future trends in high-entropy alloys, JOM (J. Occup. Med.) 65 (12) (2013) 1759–1771.
[12] M.A. Tunes, V.M. Vishnyakov, Microstructural Origins of the High Mechanical Damage Tolerance of Nbtamow Refractory High-Entropy Alloy Thin Films, Materials & Design, 2019, p. 107692.
[13] B. Murty, J. Yeh, S. Ranganathan, High-Entropy Alloys, Elsevier, 2014.
[14] D.B. Miracle, O.N. Senkov, A critical review of high entropy alloys and related concepts, Acta Mater. 122 (2017) 448–511.
[15] B. Cantor, I. Chang, P. Knight, A. Vincent, Microstructural development in equiatomic multicomponent alloys, Mater. Sci. Eng. A 375 (2004) 213–218.
[16] B. Cantor, K. Kim, P.J. Warren, Novel multicomponent amorphous alloys, Mater. Sci. Forum 386–388 (2002) 27–32.
[17] B. Cantor, Multicomponent and high entropy alloys, Entropy 16 (9) (2014) 4749–4768.
[18] E.P. George, D. Raabe, R.O. Ritchie, High-entropy alloys, Nat. Rev. Mater. (2019) 1.
[19] C.-J. Tong, M.-R. Chen, J.-W. Yeh, S.-J. Lin, S.-K. Chen, T.-T. Shun, S.-Y. Chang, Mechanical performance of the AlxCoCrCuFeNi high-entropy alloy system with multiprincipal elements, Metall. Mater. Trans. A 36 (5) (2005) 1263–1271.
[20] C. Ng, S. Guo, J. Luan, S. Shi, C.T. Liu, Entropy-driven phase stability and slow diffusion kinetics in an Al0. 5CoCrCuFeNi high entropy alloy, Intermetallics 31 (2012) 165–172.
[21] M. Lucas, G. Wilks, L. Mauger, J.A. Munoz, O.N. Senkov, E. Michel, J. Horwath, S. Semiatin, M.B. Stone, D.L. Abernathy, et al., Absence of long-range chemical ordering in equimolar fecocrni, Appl. Phys. Lett. 100 (25) (2012) 251907.
[22] C.G. Schön, T. Duong, Y. Wang, R. Arróyave, Probing the entropy hypothesis in highly concentrated alloys, Acta Mater. 148 (2018) 263–279.
[23] M.-H. Tsai, Physical properties of high entropy alloys, Entropy 15 (12) (2013) 5338–5345.
[24] Z. Lu, H. Wang, M. Chen, I. Baker, J. Yeh, C.T. Liu, T. Nieh, An assessment on the future development of high-entropy alloys: summary from a recent workshop, Intermetallics 66 (2015) 67–76.
[25] K.-H. Cheng, C.-H. Lai, S.-J. Lin, J.-W. Yeh, Recent progress in multi-element alloy and nitride coatings sputtered from high-entropy alloy targets, Ann. Chim. Sci. Mat. 31 (6) (2006) 723–736.
[26] J.-W. Yeh, S.-K. Chen, S.-J. Lin, J.-Y. Gan, T.-S. Chin, T.-T. Shun, C.-H. Tsau, S.-Y. Chang, Nanostructured high-entropy alloys with multiple principal elements: novel alloy design concepts and outcomes, Adv. Eng. Mater. 6 (5) (2004) 299–303.
[27] S. Singh, N. Wanderka, B. Murty, U. Glatzel, J. Banhart, Decomposition in multi-component AlCoCrCuFeNi high-entropy alloy, Acta Mater. 59 (1) (2011) 182–190.
[28] M.-H. Tsai, J.-W. Yeh, J.-Y. Gan, Diffusion barrier properties of AlMoNbSiTaTiVZr high-entropy alloy layer between copper and silicon, Thin Solid Films 516 (16) (2008) 5527–5530.
[29] Y. Zhang, S. Zhao, W.J. Weber, K. Nordlund, F. Granberg, F. Djurabekova, Atomic-level heterogeneity and defect dynamics in concentrated solid-solution alloys, Curr. Opin. Solid State Mater. Sci. 21 (5) (2017) 221–237.
[30] Y. Zhang, M.A. Tunes, M.L. Crespillo, F. Zhang, W.L. Boldman, P.D. Rack, L. Jiang, C. Xu, G. Greaves, S.E. Donnelly, et al., Thermal stability and irradiation response of nanocrystalline cocrcufeni high-entropy alloy, Nanotechnology 30 (29) (2019) 294004.
[31] C. Lu, L. Niu, N. Chen, K. Jin, T. Yang, P. Xiu, Y. Zhang, F. Gao, H. Bei, S. Shi, M.-R. He, I.M. Robertson, W.J. Weber, L. Wang, Enhancing radiation tolerance by controlling defect mobility and migration pathways in multicomponent single-phase alloys, Nat. Commun. 7 (2016) 13564.
[32] Z. Li, K.G. Pradeep, Y. Deng, D. Raabe, C.C. Tasan, Metastable high-entropy dual-phase alloys overcome the strength–ductility trade-off, Nature 534 (7606) (2016) 227.
[33] Y. Zhang, T.T. Zuo, Z. Tang, M.C. Gao, K.A. Dahmen, P.K. Liaw, Z.P. Lu, Microstructures and properties of high-entropy alloys, Prog. Mater. Sci. 61 (2014) 1–93.
[34] Z.J. Zhang, M.M. Mao, J. Wang, B. Gludovatz, Z. Zhang, S.X. Mao, E.P. George, Q. Yu, R.O. Ritchie, Nanoscale origins of the damage tolerance of the high-entropy alloy CrMnFeCoNi, Nat. Commun. 6 (1) (2015) 10143.
[35] C. Zhang, F. Zhang, K. Jin, H. Bei, S. Chen, W. Cao, J. Zhu, D. Lv, Understanding of the elemental diffusion behavior in concentrated solid solution alloys, J. Phase Equilibria Diffusion 38 (4) (2017) 434–444.
[36] F. Granberg, K. Nordlund, M.W. Ullah, K. Jin, C. Lu, H. Bei, L.M. Wang, F. Djurabekova, W.J. Weber, Y. Zhang, Mechanism of radiation damage reduction in equiatomic multicomponent single phase Alloys, Phys. Rev. Lett. 116 (13) (2016) 1–8.
[37] J.-W. Yeh, Physical metallurgy of high-entropy alloys, JOM 67 (10) (2015) 2254–2261.
[38] N.K. Kumar, C. Li, K. Leonard, H. Bei, S. Zinkle, Microstructural stability and mechanical behavior of FeNiMnCr high entropy alloy under ion irradiation, Acta Mater. 113 (2016) 230–244.
[39] J. Dabrowa, M. Zajusz, W. Kucza, G. Cieslak, K. Berent, T. Czeppe, T. Kulik, M. Danielewski, Demystifying the sluggish diffusion effect in high entropy alloys, J. Alloy. Comp. 783 (2019) 193–207.

[40] K.-Y. Tsai, M.-H. Tsai, J.-W. Yeh, Sluggish diffusion in Co–Cr–Fe–Mn–Ni high-entropy alloys, Acta Mater. 61 (13) (2013) 4887–4897.
[41] A. Paul, Comments on "sluggish diffusion in Co–Cr–Fe–Mn–Ni high-entropy alloys" by ky tsai, mh tsai and jw yeh, Acta Mater. 61 (2013) 4887–4897. Scripta Materialia 135 (2017) 153–157.
[42] M.A. Tunes, H. Le, G. Greaves, C.G. Schön, H. Bei, Y. Zhang, P.D. Edmondson, S. E. Donnelly, Investigating sluggish diffusion in a concentrated solid solution alloy using ion irradiation with in situ tem, Intermetallics 110 (2019) 106461.
[43] P. Franke, G. Inden, An assessment of the Si mobility and the application to phase transformations in silicon steels, Zeitschrift fur metallkunde 88 (10) (1997) 795–799.
[44] P. Franke, G. Inden, Diffusion controlled transformations in multi-particle systems, Zeitschrift fur metallkunde 88 (12) (1997) 917–924.
[45] G. Inden, Computer modelling of diffusion controlled transformations, in: A. Finel, D. Maziere, M. Veron (Eds.), Thermodynamics, Microstructures and Plasticity, Vol. 108 of NATO Science Series, Series II: Mathematics, Physics and Chemistry, 2003, Pp. 135–153, Conference of the NATO-Advanced-Study-Institute on Thermodynamics, Microstructures and Plasticity, 2002. Frejus, France, Sepp. 02–13.
[46] N. Nakada, K. Tsuboi, T. Onomoto, T. Tsuchiyama, S. Takaki, G. Inden, Thermodynamics and kinetics of solution nitriding, Calphad Comput. Coupling Phase Diagrams Thermochem. 47 (2014) 168–173, https://doi.org/10.1016/j.calphad.2014.09.006}.
[47] J. Zhang, A. Schneider, G. Inden, Initiation and growth of iron metal dusting in CO-H-2-H2O gas mixtures, Corros. Sci. 50 (4) (2008) 1020–1034, https://doi.org/10.1016/j.corsci.2007.11.021}.
[48] J. Zhang, A. Schneider, G. Inden, alpha-Fe layer formation during metal dusting of iron in CO-H-2-H2O gas mixtures, Mater. Corros. - Werkstoffe und Korrosion 54 (10) (2003) 763–769, https://doi.org/10.1002/maco.200303740}.
[49] A. Schneider, H. Viefhaus, G. Inden, Surface analytical studies of metal dusting of iron in CH4-H-2-H2S mixtures, Mater. Corros. - Werkstoffe und Korrosion 51 (5) (2000) 338–343.
[50] A. Schneider, G. Inden, H. Grabke, Q. Wei, E. Pippel, J. Woltersdorf, Effect of H2S on formation and decomposition of Fe3C and Fe5C2 under metal dusting conditions, Steel Res. 71 (5) (2000) 179–184, https://doi.org/10.1002/srin.200005710}.
[51] A. Schneider, H. Viefhaus, G. Inden, H. Grabke, E. Muller-Lorenz, Influence of H2S on metal dusting, Mater. Corros. - Werkstoffe und Korrosion 49 (5) (1998) 336–339.
[52] G. Inden, Diffusion and phase transformations in multi-component systems, in: J. Cermak, I. Stloukal (Eds.), Diffusion and Thermodynamics of Materials, Vol. 263 of Defect and Diffusion Forum, 2007, Pp. 11–20, 9th Seminar on Diffusion and Thermodynamics of Materials, 2006. Brno, Czech Republic, SEP 13-15, https://doi.org/10.4028/www.scientific.net/DDF.263.11.
[53] G. Inden, P. Neumann, Simulation of diffusion controlled phase transformations in steels, Steel Res. 67 (10) (1996) 401–407, https://doi.org/10.1002/srin.199605510}.
[54] J.R. Manning, Cross terms in thermodynamic diffusion equations for multicomponent alloys, Metall. Trans. 1 (1970) 499–505.
[55] C.G. Schon, T. Duong, Y. Wang, R. Arroyave, A proof of concept: thermodynamics of aluminum–transition metal highly concentrated alloys, J. Alloy. Comp. 781 (2019) 595–605.
[56] A. Borgenstam, A. Engström, L. Höglund, J. Ågren, DICTRA, a tool for simulation of diffusional transformations in alloys, J. Phase Equilibria 21 (3) (2000) 269–280.
[57] D. Gaertner, K. Abrahams, J. Kottke, V.A. Esin, I. Steinbach, G. Wilde, S. V. Divinski, Concentration-dependent atomic mobilities in FCC CoCrFeMnNi high-entropy alloys, Acta Mater. 166 (2019) 357–370.
[58] R. Kikuchi, Superposition approximation and natural iteration calculation in cluster-variation method, J. Chem. Phys. 60 (3) (1974) 1071–1080.
[59] S. Kejlstrup, D. Bedeux, Non-equilibrium Thermodynamics of Heterogeneous Systems, World scientific, 2008.
[60] J. Ågren, M. Hillert, Thermodynamic modeling of vacancies as a constituent, Calphad 67 (2019) 101666.
[61] R.F. Peart, Diffusion of V^{48} and Fe^{59} in vanadium, J. Phys. Chem. Solids 26 (1965) 1853–1861.
[62] R.E. Einziger, J.N. Mundy, H.A. Hoff, Niobium self-diffusion, Phys. Rev. B 17 (1978) 440–448.
[63] J.N. Mundy, S.J. Rothman, N.Q. Lam, H.A. Hoff, L.J. Nowicki, Self-diffusion in tungsten, Phys. Rev. B 18 (1978) 6566–6575.
[64] C.G. Schön, G. Inden, Concentration dependence of the excess specific heat capacity and of the thermodynamic factor for diffusion in F.C.C. and B.C.C. ordering systems, Acta Mater. 46 (1998) 4219–4231.